ELSEVIER

Journal of Fluids and Structures 26 (2010) 703–721

JOURNAL OF FLUIDS AND STRUCTURES

www.elsevier.com/locate/jfs

Combined action of transverse oscillations and uniform cross-flow on vortex formation and pattern of a circular cylinder

K.M. Lam*, P. Liu, J.C. Hu

Department of Civil Engineering, The University of Hong Kong, Pokfulam Road, Hong Kong

Received 23 July 2009; accepted 18 March 2010

Abstract

This paper attempts to study the roles of lateral cylinder oscillations and a uniform cross-flow in the vortex formation and wake modes of an oscillating circular cylinder. A circular cylinder is given lateral oscillations of varying amplitudes (between 0.28 and 1.42 cylinder-diameters) in a slow uniform flow stream (Reynolds number = 284) to produce the 2S, 2P and P+S wake modes. Detailed flow information is obtained with time-resolved particle-image velocimetry and the phase-locked averaging techniques. In the 2S and 2P mode, the flow speeds relative to the cylinder movement are less than the uniform flow velocity and it is found that initial formation of a vortex is caused by shear-layer separation of the uniform flow on the cylinder. Subsequent development of the shear-layer vortices is affected by the lateral cylinder movement. At small cylinder oscillation amplitudes, vortices are shed in synchronization with the cylinder movement, resulting in the 2S mode. The 2P mode occurs at larger cylinder oscillation amplitudes at which each shear-layer vortex is found to undergo intense stretching and eventual bifurcation into two separate vortices. The P+S mode occurs when the cylinder moving speeds are, for most of the time, higher than the speed of the uniform flow. These situations are found at fast and large-amplitude cylinder oscillations in which the flow relative to the cylinder movement takes over the uniform flow in governing the initial vortex formation. The formation stages of vortices from the cylinder are found to bear close resemblance to those of a vortex street pattern of a cylinder oscillating in an otherwise quiescent fluid at Keulegan–Carpenter numbers around 16. Vortices in the inclined vortex street pattern so formed are then convected downstream by the uniform flow as the vortex pairs in the 2P mode.

Keywords: Oscillating cylinder; Vortices; PIV

1. Introduction

When a circular cylinder moves in a fluid, large-scale vortices are formed from the roll-up of the separation shear layers. In a uniform cross-flow, a street of vortices of alternating senses of rotation is shed from the cylinder. For a circular cylinder undergoing an oscillating motion in an otherwise quiescent fluid, vortices are formed and at sufficiently long oscillation amplitudes, the vortices are shed from the cylinder. Previous studies have established a number of vortex patterns around the cylinder at different regimes depending primarily on the Keulegan–Carpenter (KC) number. The KC number is defined by $KC = U_m T/D$ or $KC = 2\pi A/D$, where D is the cylinder diameter, A the oscillation

*Corresponding author. Fax: +852 2559 5337.
E-mail address: kmlam@hku.hk (K.M. Lam).

0889-9746/$ - see front matter © 2010 Elsevier Ltd. All rights reserved.
doi:10.1016/j.jfluidstructs.2010.03.007

amplitude, T the period of oscillation and U_m the maximum velocity in the oscillation [e.g., Bishop and Hassan (1964), Williamson (1985), Lam and Dai (2002)]. The Reynolds number for this flow is usually defined as $Re_m = U_m D/\nu$, ν being kinematic viscosity of the fluid. At lower Reynolds numbers, viscous effect is important and the flow is affected additionally by the Stokes number which is defined by $\beta = D^2/\nu T$ (Tatsuno and Bearman, 1990; Lam and Dai, 2002). In fact, Re_m is the product of KC and β.

In the case of a circular cylinder made to oscillate laterally in a uniform cross-flow, Williamson and Roshko (1988) also found a number of vortex patterns which depend not only on the amplitude ratio A/D (or equivalently, KC) but also on the wavelength ratio λ/D. The wavelength λ is a measure of the displacement covered by the cylinder relative to the cross-flow during a cycle of cylinder oscillation. It is given by the product of T and the ambient flow velocity U_0 ($\lambda = U_0 T$). Notably, a "mode jump" in the wake pattern was observed when the period of cylinder oscillation changes across the "natural" vortex shedding period of a cylinder in uniform cross-flow (equivalent to $\lambda/D \approx 5$).

Most investigations on flow past a circular cylinder oscillating transversely to a flow stream refer to the mode map of Williamson and Roshko (1988) in which the 2S, 2P, and P+S vortex modes are expected in flow regimes on the (A/D, λ/D) plane. The mode map is based on observations from flow visualizations and, recently, Morse and Williamson (2009) reported another flow regime map based on fluid force measurements on a very fine grid of (A/D, λ/D). It was found that the transitions between regimes can occur sharply and there is a remarkable agreement between the shapes of the regimes from force measurements and those from flow visualizations. A new regime was found and this $2P_O$ mode is quite similar to the 2P mode except that the second vortex of each pair is much weaker than the first vortex. The study also reported phase-averaged velocity and vorticity data from particle-image velocimetry (PIV) measurements for the different vortex modes.

The motivation of the present work arises from our investigation of vortex patterns around a circular cylinder oscillating in an otherwise quiescent fluid (Lam and Dai, 2002). We have subsequently carried out time-resolved PIV measurements at KC >8 to understand the mechanisms of vortex formation and shedding for different vortex patterns. At KC between 12 and 16, the dominant vortex mode is the lateral vortex street pattern described in Williamson (1985) and Obasaju et al. (1988), but we also observed a sub-mode in which the vortex street on one side of the line of cylinder movement is inclined at about 45° to the line (Lam et al., 2010). This bears some resemblance to the P+S mode of a cylinder oscillating in a cross-flow in which the vortex pair is also convected away from the cylinder at about 45°. Therefore, we attempt to seek a connection between the vortex formation mechanisms in the two flow cases. In other words, we are interested in how the vortex formation processes of an oscillating cylinder are affected by the presence of an ambient cross-flow of relatively slow velocity, in which U_0 is of the order of U_m. Some preliminary results were reported in Liu et al. (2008) and phase-averaged PIV measurements were presented for the 2S, 2P and P+S modes. Those efforts appear to be concurrent with those of Morse and Williamson (2009) who measured the P+S mode for the first time with PIV. In this paper, we present the complete set of PIV measurement data and vortex dynamics subsequent to the preliminary work of Liu et al. (2008).

Many highly cited discovery works on flow around an oscillating cylinder [e.g., Williamson (1985)] and flow over a cylinder oscillating in a uniform cross-flow [e.g., Williamson and Roshko (1988), Ongoren and Rockwell (1988a, b)] were based on flow visualizations. At present, advances in PIV technology, in particular time-resolved PIV made possible by high-speed cameras, have provided us with the necessary temporal and spatial resolutions for the study of vortex shedding flows. The information of instantaneous or phase-averaged velocity fields enables more quantitative understanding of the vortex dynamics than flow visualization. For instance, Jeon and Gharib (2004) have reported PIV vorticity contours for the 2S and 2P modes of a circular cylinder oscillating laterally to a cross-flow. The vortex formation time was proposed in that study to explain the transition between the two modes. This paper aims to investigate in details the vortex formation processes in the different vortex modes of an oscillating cylinder in a cross-flow through phase-averaged PIV measurements.

In this study, we aim at a highly two-dimensional flow geometry in the experimental set-up and mainly focus on the coherent vortex patterns on the two-dimensional plane. Fine flow structures in the span-wise direction of the cylinder and three-dimensional flow features are always present at the present Reynolds number range but their investigation is outside the scope of this paper. The effect of the Stokes number is also not studied. It is believed that in the presence of an ambient cross-flow the viscous effect has a reduced significance on the oscillating cylinder.

2. Experimental techniques

Experiments were carried out in a water tank facility measuring 1.8 m long and 1.2 m wide and with water filled to 0.5 m depth. At mid-length of the tank, a transparent circular cylinder of $D = 15$ mm was mounted vertically on a

Table 1
Flow parameters of experiments. $D = 15\,\text{mm}$, $U_0 = 17\,\text{mm/s}$, $\text{Re} = U_0 D/\nu = 284$.

	A/D	λ/D	KC	U_0/U_m	T (s)	$\text{Re}_m = U_m D/\nu$
"2S"	0.28	5.52	1.76	3.14	4.90	90
"2P"	0.75	5.52	4.71	1.17	4.90	241
"P+S"	1.42	3.10	8.92	0.35	2.75	814

traversing table which was placed above the tank. The clearance of the cylinder end from the bottom of the tank was about 1 mm and the aspect ratio of the cylinder was larger than 33. The table and the cylinder were given forced sinusoidal oscillations in the lateral direction at given amplitudes and periods with a motor-crank mechanism and a stepper motor. A uniform flow stream at $U_0 = 17\,\text{mm/s}$ was produced along the tank by circulating water from one end to the other with a pump. A contraction section was installed to improve the uniformity and smoothness of the flow stream. This has been checked with PIV on the measurement plane. In the region downstream of the cylinder up to $x/D = 8$ and within $y/D = \pm 4$, 90% of the flow vectors had U within $17.0 \pm 0.5\,\text{mm/s}$ and V within $\pm 0.2\,\text{mm/s}$. The axial turbulence intensity was about 0.05. The coordinates (x, y) are downstream and lateral to the centre of the cylinder in its neutral position and (U, V) are the corresponding components of the velocity vectors.

Time-resolved PIV measurements were made at three flow cases corresponding to three points on the $(A/D, \lambda/D)$ plane. Their values and other flow parameters are listed in Table 1. The parameters include KC, Reynolds number, $\text{Re}_m = U_m D/\nu$, and the ratio of velocities, U_0/U_m. It is worth noting that the velocity ratio can relate the wavelength ratio and KC through $\lambda/D = \text{KC} \times U_0/U_m$. It should also be noted that in all cases, the same ambient flow velocity at $U_0 = 17\,\text{mm/s}$ was used. The cross-flow Reynolds number thus had a constant value, $\text{Re} = U_0 D/\nu = 284$. The three flow cases were decided based on the mode map of Williamson and Roshko (1988) in which the 2S, 2P and P+S modes are expected. However, according to the latest mode map of Morse and Williamson (2009), the second flow case falls into the regime of the $2P_O$ mode.

The time-resolved PIV system comprised of three parts, namely, a 6-W Argon-ion laser with light sheet optics, a high-speed CCD camera (model PCO 1200hs) with 1280×1024 pixel resolution, and a PIV analysis software (Dantec Dynamic Studio). Neutrally buoyant polyamid particles of 50 μm nominal diameter were used to seed the water. The laser sheet illuminated a horizontal plane of the flow at mid-depth and the flow images were taken from the camera viewing from below the transparent bottom of the tank. The camera was set at a speed of 100 image/s to capture a time sequence of particle images. Particle images recorded on two consecutive images were analysed for an instantaneous PIV snapshot. The analysis was based on the spatial cross-correlation algorithm of Willert and Gharib (1991) but with adaptive and multi-pass interrogation windows. In the final iteration, PIV vectors are obtained on interrogation areas of size 32 pixels × 32 pixels and with 50% overlap. Thus, the two-dimensional velocity field at each time instant consisted of 79×63 vectors of U and V. For each flow case, PIV snapshots were taken for 30 cycles of lateral oscillation of the cylinder and there were 490 or 275 snapshots in each cycle. The PIV system thus provided sufficiently fine temporal resolution for the investigation of vortex formation and evolution processes. From the velocity vectors, span-wise vorticity, ζ, was computed from the fluid circulation (Lam and Leung, 2005). Experimental uncertainties in determining the velocities and span-wise vorticity were estimated to be 5% and 7%, respectively.

The phase-lock averaging technique has proven to be a useful tool to investigate quasi-periodic flows such as vortex shedding flow; see, for example, Reynolds and Hussain (1972), Cantwell and Coles (1983), and Govardhan and Williamson (2001). Our PIV experiments produced velocity snapshots at very fine resolution in order of hundreds of images per oscillation cycle. To make full use of the data, a modified phase-averaging procedure was adopted. For each selected phase of the cylinder oscillation cycle, an interval Δt was chosen and several sequential velocity snapshots within this interval were selected to represent the pattern at this phase. All PIV snapshots at this phase were then averaged over 30 cycles of cylinder oscillation to obtain the phase-averaged velocity field at the selected phase, from which the coherent vorticity field at this phase was also computed. The fine temporal resolution of our PIV data enabled us to carry out phase-lock averaging at many successive phases of fine intervals in a typical cycle of cylinder oscillation.

3. Results and discussion

Compared with the case of an oscillating cylinder in an otherwise quiescent fluid, vortex formation in the wake of the cylinder in the presence of a uniform cross-flow is highly repetitive and regular. In our three flow cases, vortex

formation was found to be highly synchronized with the cylinder motion. As mentioned previously, we chose the three flow cases according to the mode map of Williamson and Roshko (1988) to investigate the 2S, 2P and P+S modes. We have tried to vary mainly the oscillation amplitudes with a small value of λ as listed in Table 1. Essentially, the 2S mode has two single vortices shed per cycle of cylinder oscillation, and in the 2P mode two pairs of vortices are formed during a cycle. The P+S mode is an asymmetric mode in which one pair of vortices and one single vortex are formed in one cycle. These modes of vortex pattern can last for at least hundreds of cylinder cycles. However, the latest mode map of Morse and Williamson (2009) suggests that our second flow case falls into the regime of the newly discovered $2P_O$ mode. For illustration, Fig. 1 shows the coherent vorticity fields of the three modes when the cylinder is at one extreme position of its oscillation. The vorticity is computed from the phase-averaged velocity field at that phase and shown in the nondimensional form of $\zeta D/U_0$.

3.1. Inclined vortex street and P+S mode

We first explore the similarities between the P+S mode and the inclined vortex street of a circular cylinder oscillating in an otherwise quiescent fluid. Fig. 2 shows some instantaneous PIV snapshots for the latter case at KC = 16. This case corresponds to $A/D = 2.55$ and $\lambda/D = 0$. Detailed discussion of the vortex pattern is recently reported in Lam et al. (2010) in which a fuller set of PIV results are presented. In the absence of a uniform cross-flow, the vortex pattern is found to be less regular and periodic, and phase-locked averaging is not carried out on the PIV data. However, the key stages of vortex formation and development can be observed in Fig. 2. While all vortices are convected to the vortex street located to the right of the line of cylinder movement in the figure, each vortex is actually first formed from the roll-up of the shear layer on the left side of the cylinder at the start of every cylinder stroke (Fig. 2(b)). During the stroke, the vortex grows with the feed of vorticity from the shear layer. Near the middle of the stroke, a vortex of the opposite sense of rotation is shed from the right side of the cylinder (Fig. 2(c, d)). Connected with this shedding, the vortex on the left shear layer moves rightwards around the leeward side of the cylinder surface. The rightward migration of the vortex continues due to the presence of a rightwards-flowing biased flow stream. When the cylinder traverses its next stroke, the vortex is eventually brought to the right cylinder surface and vorticity is fed to it from the right-side shear layer instead (e.g., Fig. 2(b)). The vortex grows to maturity and is subsequently shed into the wake to the right of the cylinder near the middle of the stroke. Fig. 2(d) suggests that shedding of the vortex seems to be triggered by an interaction with the preceding vortex of the opposite sense of rotation. When the cylinder travels past the latter vortex, the vortex developing on the right side of the cylinder undergoes some stretching (Fig. 2(c)). The main and trailing portion of the vortex is induced to be shed and pairs up with the preceding vortex while a smaller part remains attached to the advancing cylinder (Fig. 2(e)).

Jeon and Gharib (2004) suggested the use of an equivalent travelling distance for the formation time of a vortex for shedding from a circular cylinder. The vortex distance was defined as the relative distance that the flow passes over the cylinder during the formation time. It was suggested that around a time of $4.8D$, a vortex grows to reach a critical circulation and shedding occurs. For an oscillating cylinder, the vortex street pattern occurs at $8 < \mathrm{KC} < 16$. As shown in Fig. 2, when a typical vortex develops from initial roll-up to shedding, the cylinder moves through $1\frac{1}{2}$ cylinder strokes or $3A$ approximately. This distance is between $3.8D$ and $7.6D$ for $8 < \mathrm{KC} < 16$. As higher KC, the cylinder strokes are longer and more than one pair of vortices are formed for one cylinder oscillation cycle.

In the presence of a uniform cross-flow, the relative distance which the fluid passes over the oscillating cylinder is increased from the no flow case. Fig. 3 shows the phase-averaged vorticity fields at 16 successive phases of a cylinder oscillation cycle for our P+S mode at $A/D = 1.42$ and $\lambda/D = 3.10$. It is noted that the pattern of the vortex pair in the P+S mode bears close resemblance to the inclined vortex street in Fig. 2. To study the combined action of the lateral cylinder oscillation and the uniform flow stream, we also plot in Fig. 3 the phase-averaged velocity vectors relative to the moving cylinder. It can be observed when the cylinder moves through its neutral position, fluid flows past it almost along the lateral direction. This is due to the low velocity of the uniform flow velocity as compared to the cylinder oscillating velocity, $U_0/U_m = 0.35$.

In Fig. 3, when the cylinder moves downwards from its uppermost position, it drags along with it the counterclockwise vortex of positive vorticity on the downstream side (or the right side of the cylinder as shown in Fig. 3). This vortex, denoted by P1, is formed during the previous upward stroke. The relative velocity vectors in Fig. 3(d–f) show that fluid passes the cylinder in an almost lateral direction during the middle of the cylinder stroke. The flow physics is very similar to that in Fig. 2 for $U_0 = 0$. There is a separation shear layer developed on the upstream side (left side) of the cylinder. The roll-up of the shear layer gives rise to a clockwise vortex N1 (of negative vorticity) which can be observed attached to the upper left side of the cylinder in Fig. 3(e–g). Similar to the case of $U_0 = 0$ in Fig. 2, vortex N1 has migrated to the right side of the cylinder as the cylinder moves to its lowermost position. While this

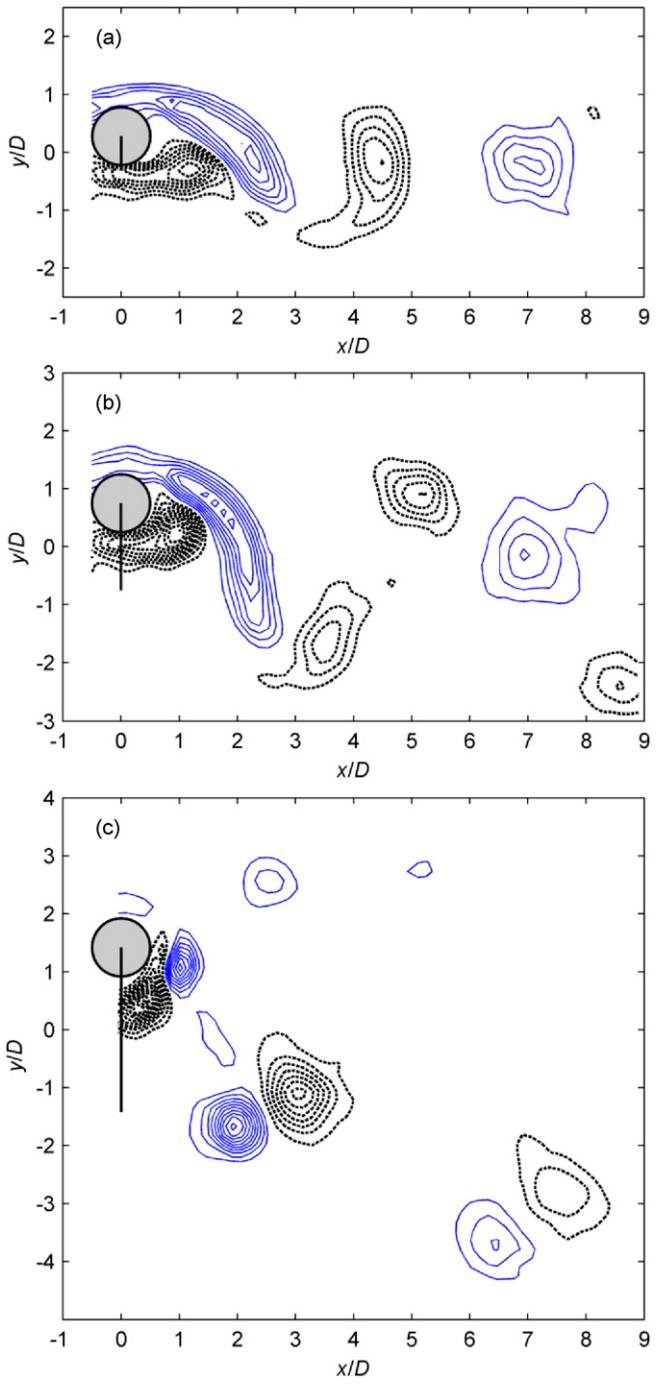

Fig. 1. Phase-averaged vorticity field when cylinder reaches its extreme position for our three flow cases of vortex modes: (a) 2S; (b) 2P; (c) P+S. Vorticity contours at $\zeta D/U_0=\{\pm 0.35,\ \pm 0.7,\ \pm 1.05,\ \ldots\}$.

vortex migration is brought about by the biased flow stream in Fig. 2, it is now facilitated by the uniform flow stream in Fig. 3. The migration of vortex N1 to the downstream side of the cylinder in Fig. 3(h) also cuts off the mature vortex P1 from its shear layer and thus triggers its shedding from the cylinder.

Now the cylinder reverses its movement and traverses its upward stroke from Fig. 3(i) onwards. Vortex N1 is brought across the returning cylinder and becomes attached to the downstream side of the cylinder. It continues to grow with

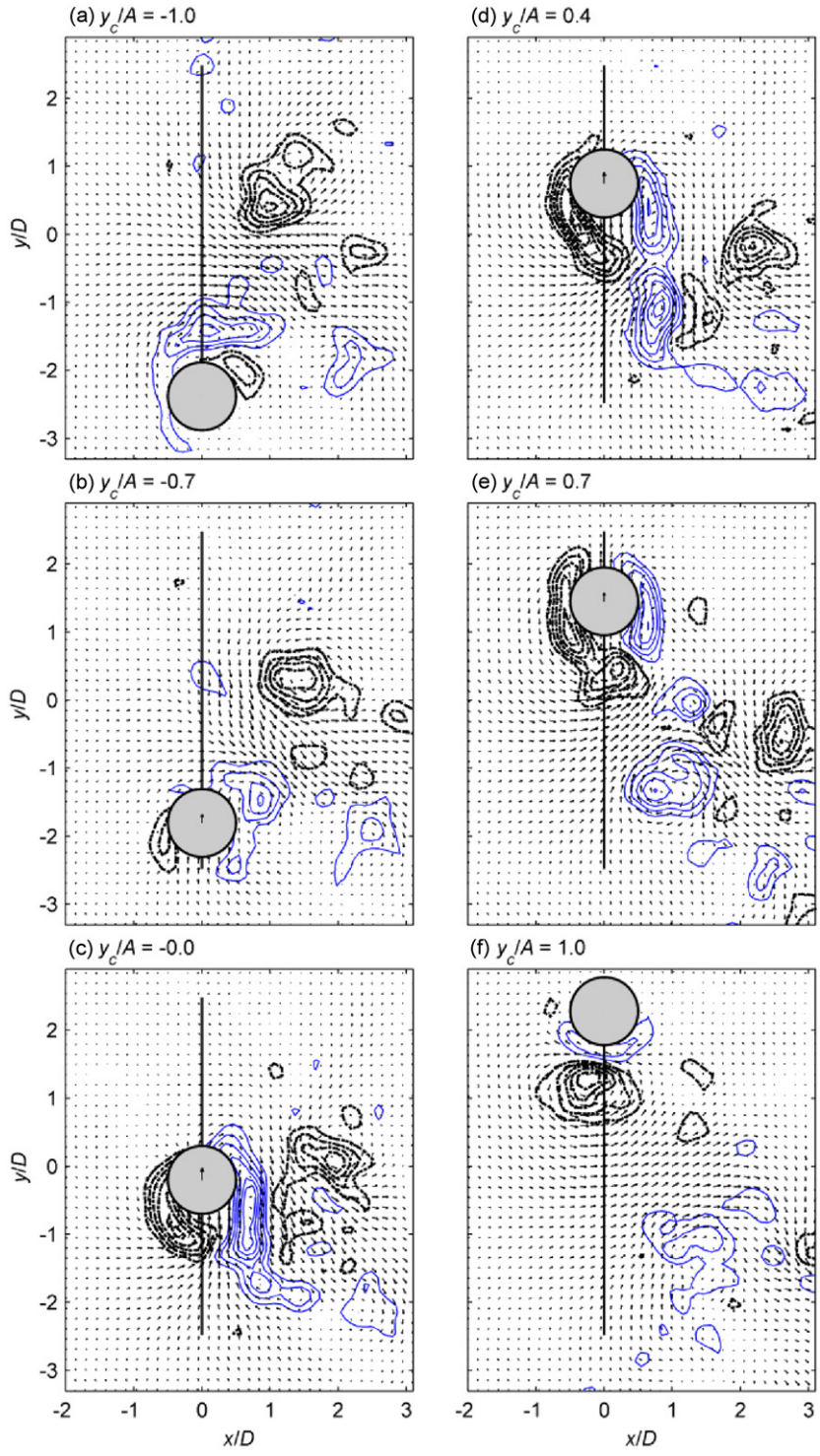

Fig. 2. Instantaneous velocity vectors and vorticity fields at selected phases of circular cylinder oscillating in otherwise quiescent water. Inclined vortex street pattern at KC = 16. Vorticity contours at $\zeta D/U_m = \{\pm 0.8, \pm 1.6, \pm 2.4, \ldots\}$. Phases denoted by lateral displacements of cylinder centre, y_c: (a) $y_c/A = -1.0$; (b) $y_c/A = -0.7$; (c) $y_c/A = -0.0$; (d) $y_c/A = 0.4$; (e) $y_c/A = 0.7$; (f) $y_c/A = 1.0$.

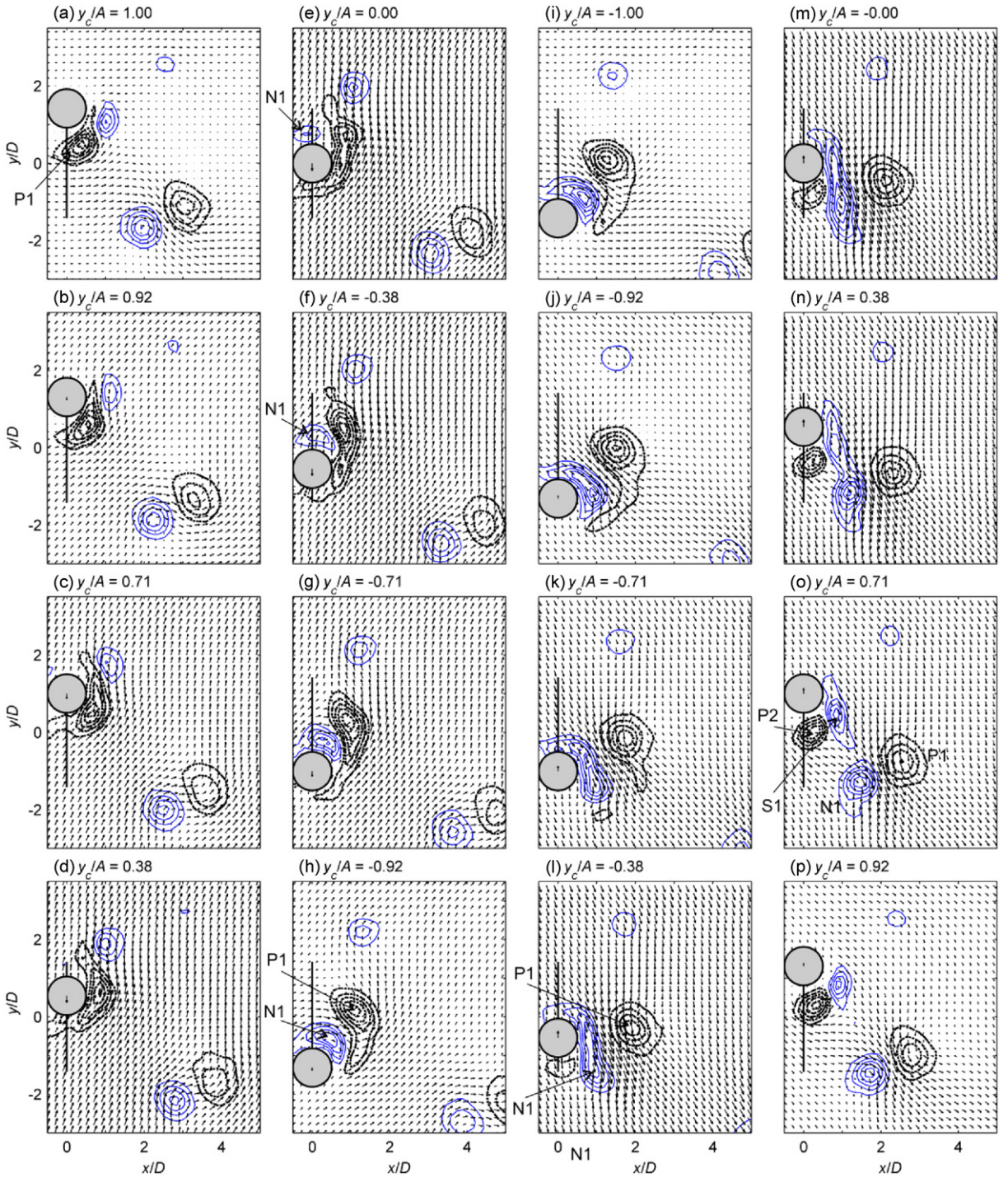

Fig. 3. Phase-averaged velocity vectors and vorticity fields at 16 successive phases of cylinder movement in P+S mode. Vorticity contours at $\zeta D/U_m = \{\pm 0.05, \pm 0.1, \pm 0.15, \pm 0.2, \ldots\}$. Velocity vectors relative to moving cylinder: (a) $y_c/A = 1.00$; (b) $y_c/A = 0.92$; (c) $y_c/A = 0.71$; (d) $y_c/A = 0.38$; (e) $y_c/A = 0.00$; (f) $y_c/A = -0.38$; (g) $y_c/A = -0.71$; (h) $y_c/A = -0.92$; (i) $y_c/A = -1.00$; (j) $y_c/A = -0.92$; (k) $y_c/A = -0.71$; (l) $y_c/A = -0.38$; (m) $y_c/A = -0.00$; (n) $y_c/A = 0.38$; (o) $y_c/A = 0.71$; (p) $y_c/A = 0.92$.

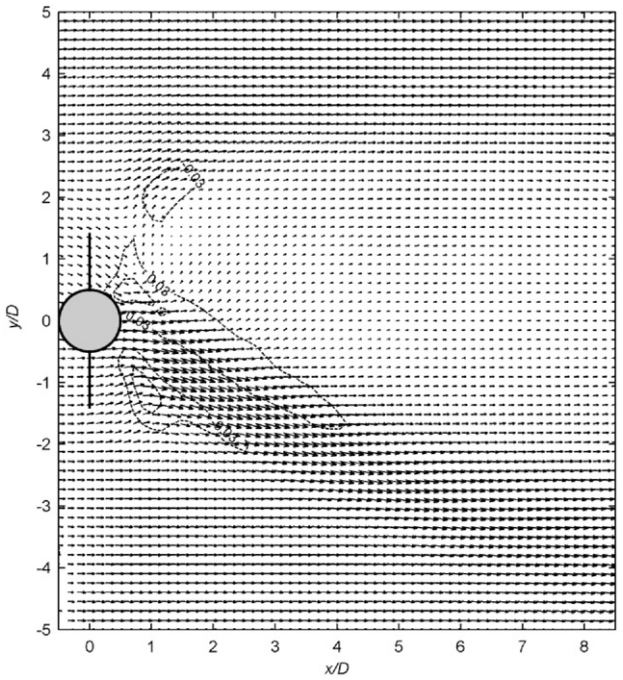

Fig. 4. Mean flow vectors in P+S mode, with mean vorticity contours of $\zeta D/U_m$.

vorticity supplied by the shear layer on this right side of the cylinder. When the cylinder passes its neutral position in Fig. 3(l, m), vortex N1 is stretched by the downstream vortex P1. This mechanism is the same as that in Fig. 2(c, d) and leads to the detachment of the larger and trailing part of N1 from the cylinder as a shed vortex. The shedding process is completed in Fig. 3(n) and the leading part of N1 remains attached to the departing cylinder and we name this part as S1.

During the upward stroke of the cylinder, a new counterclockwise vortex is rolled up from the upstream side of the cylinder. In Fig. 3(n–p), this vortex P2 is migrated to the downstream side of the cylinder which is approaching its uppermost position. As the cylinder moves downwards in the next stroke in Fig. 3(b), vortex P2 starts to be brought across the returning cylinder while the single vortex S1 is shed behind. Therefore the P+S mode is completed for one cylinder oscillation cycle. In the case of $U_0 = 0$, the single vortex is not observed in Fig. 2. This is probably because the remaining part of the vorticity region (after the shedding of vortex N1) cannot be convected away from the cylinder in the absence of a uniform flow stream in Fig. 2(e). When the cylinder reverses its movement, it impinges onto the remaining vorticity region and leads to the disintegration of the latter.

While we observe great similarities between the formation mechanism of the P+S mode in Fig. 3 and that of the inclined vortex street in Fig. 2, the cylinder in the former case undergoes much smaller amplitudes of lateral oscillation at $A/D = 1.42$, or equivalently KC = 8.92 only. The formation of a vortex in the vortex pair occurs for about $1\frac{1}{2}$ cylinder strokes and this is $4.3D$ in Fig. 3, while the distance is $7.6D$ in Fig. 2. However, we suggest that the vortex formation distance should be taken as the distance which the cylinder moves relative to the flow during the instant from the initial formation of a vortex to its shedding. In the presence of a uniform cross-flow, the relative flow velocity to the cylinder is always higher than in the case of $U_0 = 0$. Thus, the actual vortex formation distance for vortex N1 or P1 in Fig. 3 is longer than $4.3D$. We believe that this adjustment should also be considered in the use of the wavelength ratio λ/D.

The P+S mode is an asymmetric mode and this is particularly so in our case of a low value of $U_0/U_m = 0.35$. Fig. 4 shows the time-averaged mean velocity field in the wake of the cylinder. We can observe that the mean velocity field is also asymmetric and there exists a jet-like flow stream inclined to one side from the direction of the uniform flow stream. This flow stream is coincident with the trajectory of the vortex pair and bears some similarities to the biased secondary flow stream observed for the vortex street pattern of a cylinder oscillating in an otherwise quiescent flow (Williamson, 1985; Lam et al., 2010). The mean vorticity field computed from the velocity vectors is also shown in the figure.

The trajectories of the vortices in Fig. 3 and their peak vorticity levels are found using the techniques described in Lam (2009). The P+S mode is clearly observed in the vortex trajectories in Fig. 5(a). The convection of the vortex pair in the P+S mode follows a path which is inclined at about 30° to the direction of the uniform flow while the single

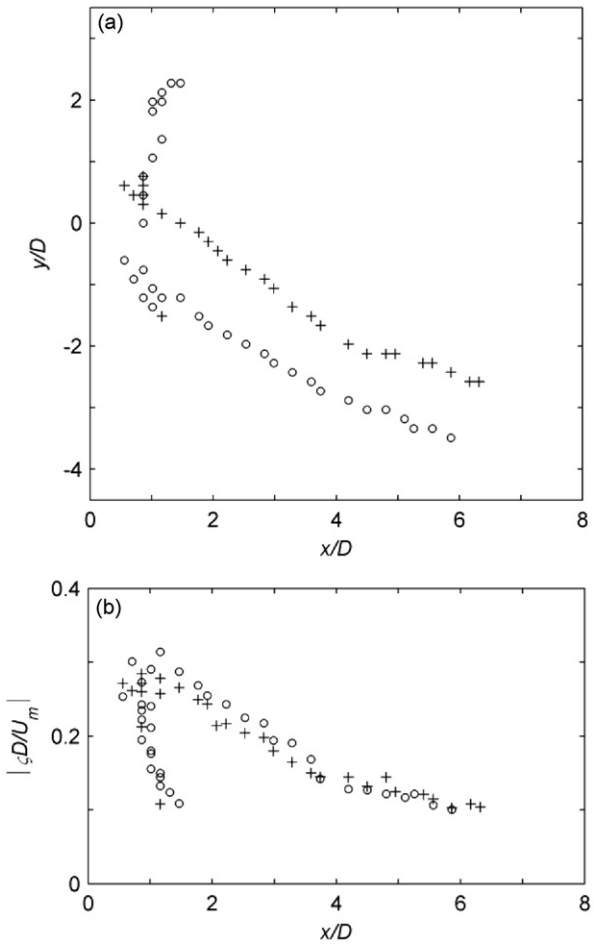

Fig. 5. Convection paths and peak vorticity levels of vortices in P+S mode: (a) locations of peak vorticity; (b) magnitudes of peak vorticity. Symbols: +, counterclockwise vortex of positive vorticity; ○, clockwise vortex of negative vorticity.

vortex is convected along a less oblique path. Fig. 5(b) compares the magnitudes of the peak vorticity levels of the three vortices. The vorticity levels are shown in the nondimensional form of $\zeta D/U_m$ and the normalization using U_m is for comparison with other vortex modes. These measures of vortex strengths drop with downstream distance but it is evident that the strengths of the clockwise vortex N1 in the vortex pair are the same or even slightly higher than that of its counterclockwise partner P1. This is a bit surprising because the single vortex is also rotating clockwise, although its peak levels of negative vorticity are much lower than either vortex of the vortex pair. Although Fig. 5 only compares the peak vorticity levels, it is likely that there is a net excess of negative vorticity in the wake. We have also tried to integrate the mean vorticity field in Fig. 4 in the cylinder wake. A small negative value is indeed obtained for the area-averaged mean vorticity at $\zeta D/U_m \approx -0.0005$, although this small magnitude might be affected by experimental uncertainties. In the studies of a lift-generating body including an inclined flat plate at high incidence and a rotating circular cylinder, Lam and Leung (2005) and Lam (2009) argued that a mean lift is connected with a net excess of fluid circulation in the wake. If we accept this argument, the circular cylinder in the P+S mode would be under a mean fluid force in the lateral direction. We have not made force measurements but we find that there appears a small mean component in the lift measurement data of Morse and Williamson (2009) for the asymmetric P+S mode.

3.2. 2S and 2P modes

To study the 2S and 2P modes while keeping the uniform cross-flow slow, we choose our flow cases at a low value of $\lambda/D = 5.52$. At a small amplitude of lateral cylinder oscillations at $A/D = 0.28$ (KC = 1.76), we observe the 2S mode,

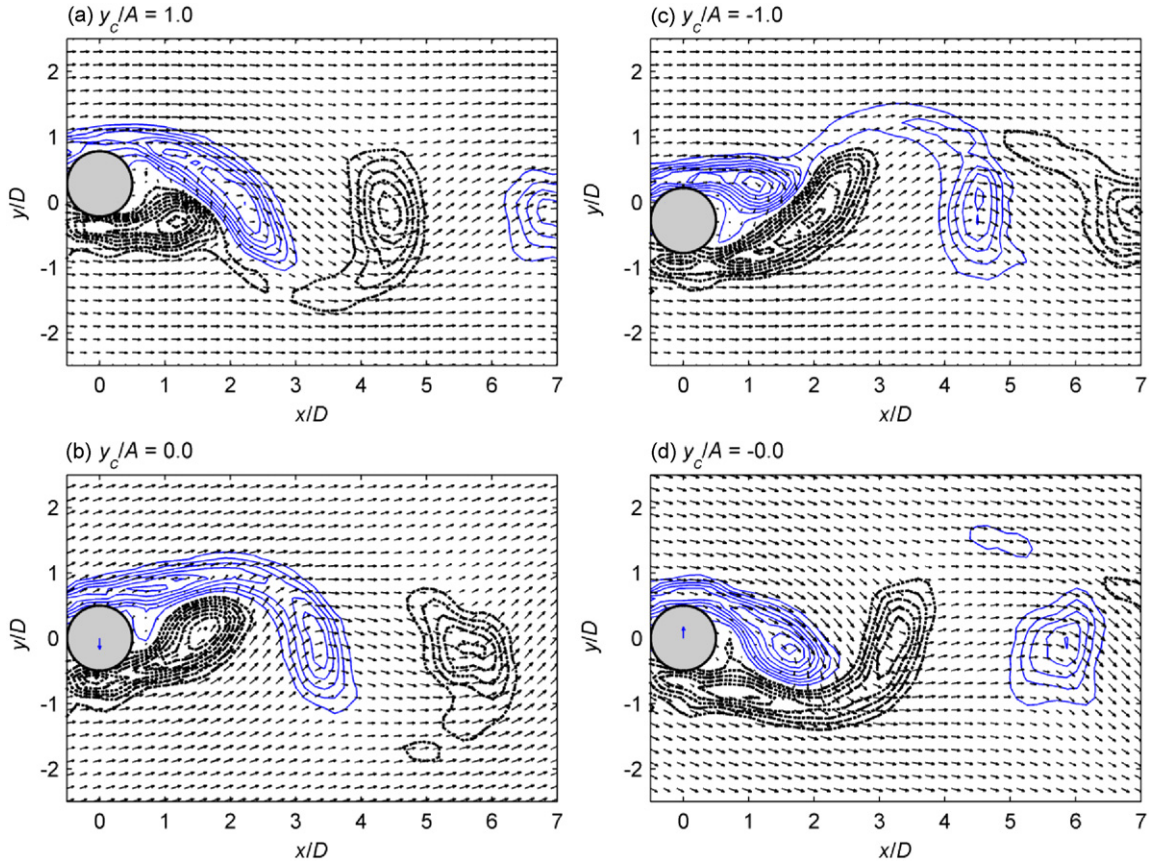

Fig. 6. Phase-averaged velocity vectors and vorticity fields at selected phases of cylinder movement in 2S mode. Velocity vectors relative to moving cylinder. Vorticity contours at $\zeta D/U_m = \{\pm 0.1, \pm 0.2, \pm 0.3, \ldots\}$: (a) $y_c/A = 1.0$; (b) $y_c/A = 0.0$; (c) $y_c/A = -1.0$; (d) $y_c/A = -0.0$.

while as the amplitude increases to $A/D = 0.75$ (KC = 4.71), we expect the 2P mode from the mode map of Williamson and Roshko (1988). Figs. 6 and 7 shows the phase-averaged PIV results of these two flow cases, respectively. It is evident that the vortex formation process undergoes a mode transition when the amplitude of cylinder oscillations changes between the low and high values.

The 2S mode in Fig. 6 is highly symmetrical and thus we only show the phase-averaged flow at a few phases of cylinder oscillation. In every cylinder oscillation cycle, two vortices of opposite signs of rotation are shed alternatively from the cylinder, resulting in a nice vortex street in the wake. Owing to the small amplitudes of cylinder oscillation, the cylinder always moves with slow lateral velocities bounded by $U_m < 0.31 U_0$ ($U_0/U_m = 3.14$). Even when the cylinder travels past its neutral position with its maximum lateral velocity U_m (e.g., in Fig. 6(b)), there is no significant effect on the relative flow approaching directions to the cylinder (that has been observed in the P+S mode in Fig. 3). However, we can observe in Fig. 6(b, d) that as the cylinder moves from one extreme position towards the neutral position, it seems to induce the region of concentrated vorticity on the frontal side of its movement to migrate towards the central line of the wake. This phenomenon is illustrated by the trajectories of vortex centres in Fig. 8. The migration of the locations of peak positive or negative vorticity towards the wake centerline occurs within $x/D < 1.5$. Farther downstream, the 2S vortices of opposite signs of rotation both lie almost on the wake centerline. This aspect of the vortex street pattern differs from that of a stationary cylinder in uniform cross-flow in which the alternating vortices were found to convect downstream along parallel paths at $y/D \approx \pm 0.5$ (Cantwell and Coles, 1983; Lam, 2009). The contra-rotating vortices of the 2S mode are found to possess same strengths at corresponding downstream locations and the results are not shown for brevity.

In our opinion, the vortex pattern would remain in the symmetric and relatively simple 2S mode, provided that the action of the relative flow velocities caused by the lateral movement of the cylinder is small compared with that of the uniform cross-flow and that the period of the oscillation does not exceed the natural vortex formation distance of $4.8D$

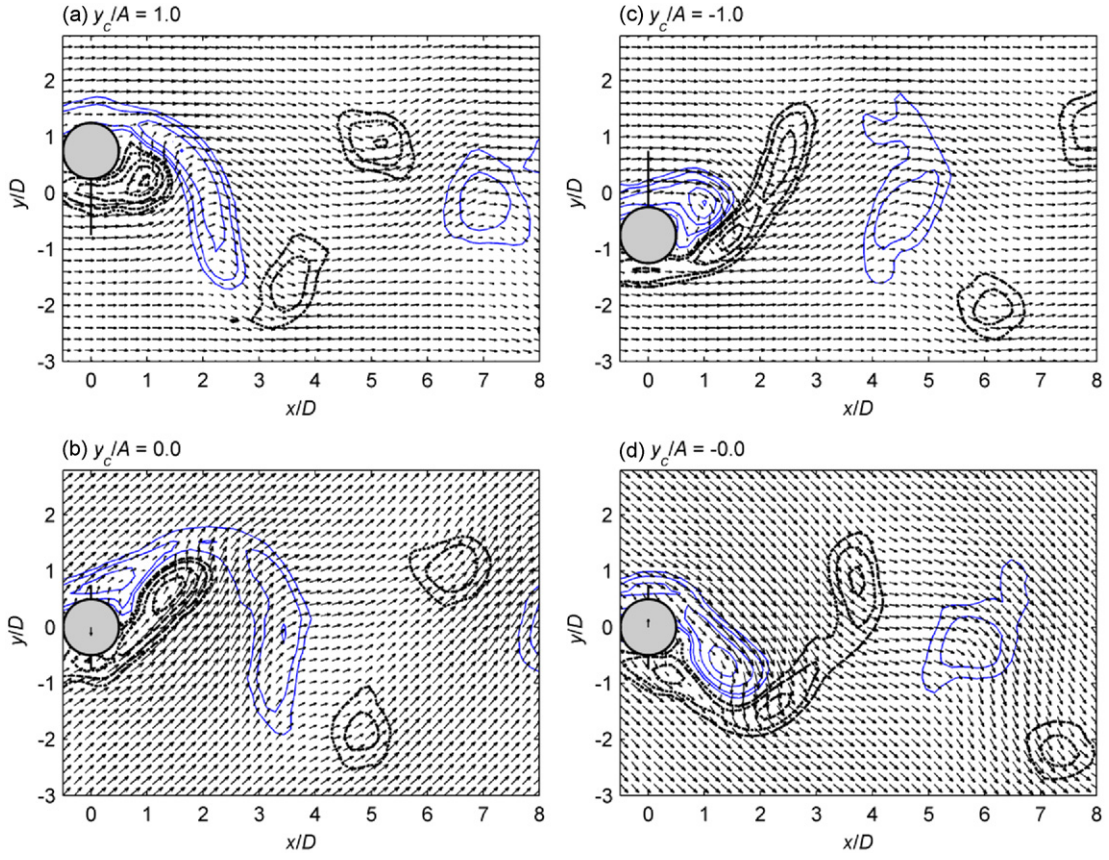

Fig. 7. Phase-averaged velocity vectors and vorticity fields at selected phases of cylinder movement in 2P mode. Velocity vectors relative to moving cylinder. Vorticity contours at $\zeta D/U_m = \{\pm 0.05, \pm 0.1, \pm 0.2, \pm 0.3, \ldots\}$: (a) $y_c/A = 1.0$; (b) $y_c/A = 0.0$; (c) $y_c/A = -1.0$; (d) $y_c/A = -0.0$.

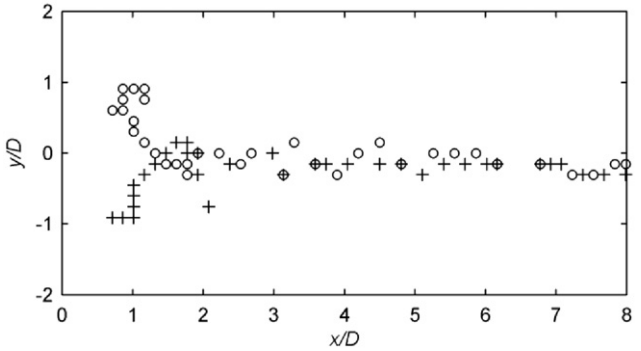

Fig. 8. Vortex convection paths as shown locations of peak vorticity levels in 2S mode: +, counterclockwise vortex of positive vorticity; ○, clockwise vortex of negative vorticity.

by a factor of about two. According to the mode map of Williamson and Roshko (1988), the 2S mode can occur only when the circular cylinder oscillates with low amplitudes and at frequencies close to the natural shedding frequency of a stationary cylinder. Our conjecture is consistent with the region of the 2S mode in the mode map.

We now return to Fig. 7 where we expect to observe the 2P mode. The amplitudes of cylinder oscillation are almost three times those of the 2S mode in Fig. 6. This leads to a higher value of U_m at $U_0/U_m = 1.17$ and thus we can observe from the relative velocity vectors in Fig. 7(b, d) that when the cylinder travels past its neutral position with lateral

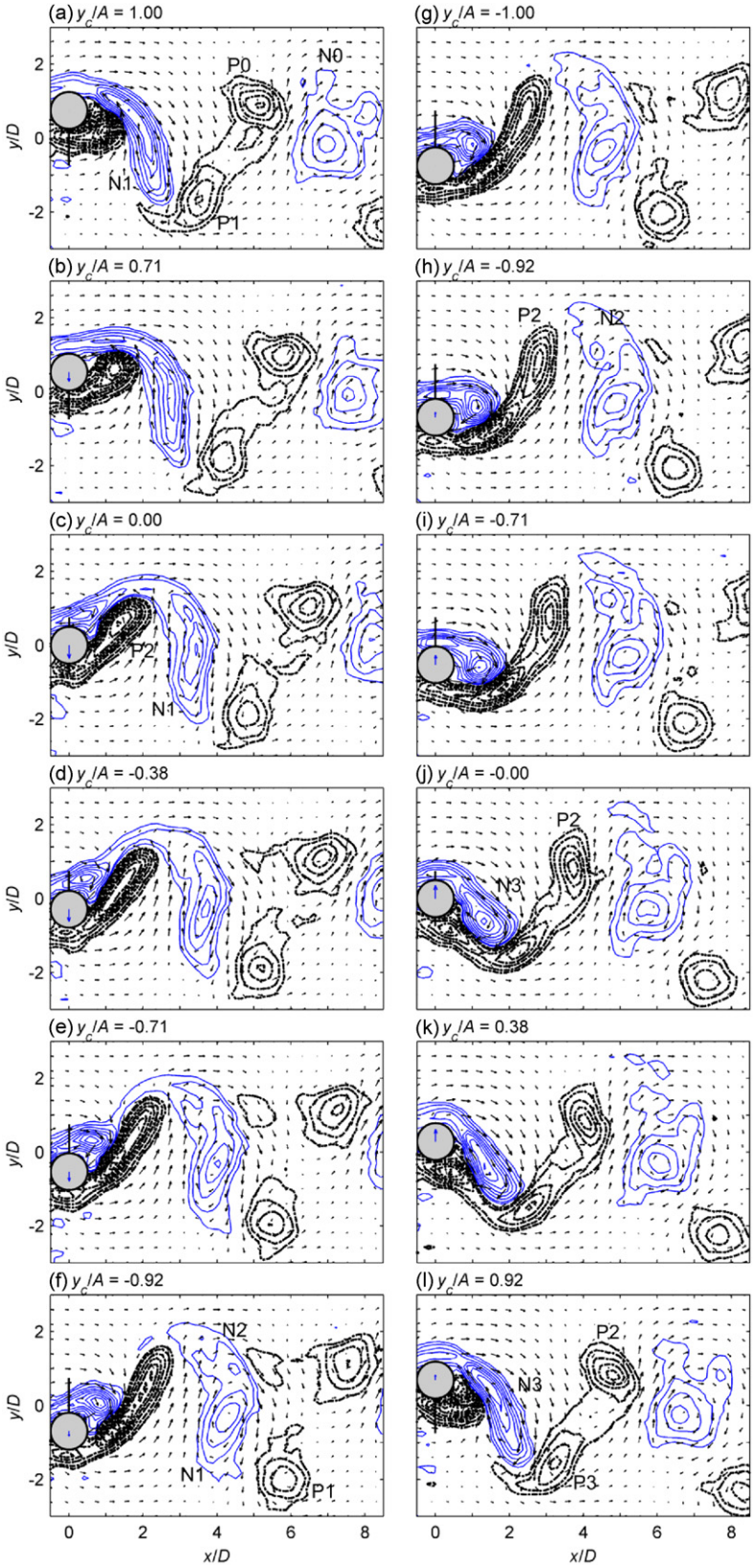

Fig. 9. Evolution of vortex patterns at successive phases of cylinder movement in 2P mode: phase-averaged vorticity fields and velocity vectors as appeared to observer travelling with vortices convecting downstream at $0.8U_0$. Vorticity contours at $\zeta D/U_m = \{\pm 0.025, \pm 0.05, \pm 0.1, \pm 0.15, \ldots\}$: (a) $y_c/A = 1.00$; (b) $y_c/A = 0.71$; (c) $y_c/A = 0.00$; (d) $y_c/A = -0.38$; (e) $y_c/A = -0.71$; (f) $y_c/A = -0.92$; (g) $y_c/A = -1.00$; (h) $y_c/A = -0.92$; (i) $y_c/A = -0.71$; (j) $y_c/A = -0.00$; (k) $y_c/A = 0.38$; (l) $y_c/A = 0.92$.

velocity U_m, fluid approaches the cylinder at a noticeably inclined direction to that of the uniform flow stream. The two regions of vorticity concentration at either side of the cylinder are observed to sway sideways to align with that inclined direction. Of course, this swaying effect can also be explained by the lateral movement of the cylinder relative to the shear-layer vorticity regions which are already some distances from the moving cylinder.

In Fig. 9, detail stages of vortex development in our 2P mode are shown by the phase-averaged flow fields at some selected phases of the cylinder oscillation cycle. The uniform flow stream past the cylinder leads to regions of concentrated vorticity rolled up from the shear layers but the development of these shear-layer vortices is affected by the large lateral movement of the cylinder during a cylinder stroke. Thus, when the cylinder reaches its extreme position, the region of concentrated vorticity is significantly elongated and lying at an inclined direction to the uniform flow stream as compared to a stationary cylinder or a cylinder oscillating at smaller amplitudes in the 2S mode. Similar to the 2S mode in Fig. 6, it is observed in Fig. 9(a–c) and (g–i) that as the cylinder moves from one extreme position towards its neutral position, it brings along with its movement the shear layer on its trailing side and the associated elongated region of concentrated vorticity towards the newly rolled up vortex on the frontal side of the cylinder. This further stretches the elongated region of concentrated vorticity. In Fig. 9(j), when the cylinder moves past its neutral position in the upward stroke, this stretching triggers the separation of the downstream part of the elongated region of concentrated vorticity to become a shed vortex. This shed vortex, which we denote by P2, is located at $y/D \approx 0.8$ which corresponds very close to the extreme lateral displacement of the cylinder at $A/D = 0.75$. When the cylinder moves farther upwards (Fig. 9(k, l)), interaction of the clockwise vortex N3 from the upper shear layer with the trailing part of the elongated region of positive vorticity leads to the shedding of the later as another counterclockwise vortex P3 which is located below the wake centerline. Subsequent developments of these vortices P2, P3 and N3 from Fig. 9(l) onwards are followed by vortices P0, P1 and N1, respectively, in Fig. 9(a).

The phase-averaged PIV results of Morse and Williamson (2009) also show evidence of breaking up of the elongated region of concentrated vorticity into two successive vortices of the same sense of rotation in the 2P mode. However, when the cylinder traverses its downward stroke in Fig. 9(a–g), the region of concentrated negative vorticity, N1, does not show very clear breaking. When we compare Fig. 9(c) with (j), the region N1 is stretched to a lesser extent when the cylinder moves downwards past its neutral position than the regions of P2 and P3 when the cylinder moves upwards. This may be because in Fig. 9(c), the counterclockwise vortex P2 does not penetrate as deeply into the opposite region of concentrated vorticity as the vortex N3 does in Fig. 9(j). Nevertheless in Fig. 9(c), the vorticity contours within N1 still exhibit a shallow valley of low levels near the middle of the elongated region. When the cylinder continues to move downwards in Fig. 9(d–g), there are evidences of some tendency of N1 to split into two regions, which we denote as N1 and N2 in Fig. 9(f), but the later region N2 is not well-defined. Furthermore, the location of the peak vorticity in N1 always remains just below the wake centerline and does not extend much farther laterally as vortex P2.

Over one cylinder oscillation cycle in Fig. 9, two counterclockwise vortices, such as P1 and P2, are shed, as well as a clockwise vortex, N1, which may be counted as two not fully separated vortices, N1 and N2. In Fig. 9, we also plot the flow vectors as appeared to an observer travelling with the vortices. These vectors are obtained by subtracting $0.8U_0$ from the velocity vectors in the stationary laboratory frame, $0.8U_0$ being the assumed convection speed of the vortices (Cantwell and Coles, 1983). It is then evident, for instance, in Fig. 9(f), that P1 and N1 form a vortex pair in the lower side of the wake and fluid is induced to flow between them in the outward direction. The following vortex pair on the lower side of the wake consists of P3 and N3 (Fig. 9(j)). On the upper side of the wake, we may say that P2 and the not well-defined N2 form a vortex pair in Fig. 9(h) and there is fluid induced to flow between them. In Fig. 9(a), we can observe the preceding vortex pair of P0 and N0.

Fig. 10 shows the locations and magnitudes of peak vorticity levels in Fig. 9. The counterclockwise vortices (of positive vorticity) are clearly centred at locations of large lateral distances on either side of the wake centerline. The main clockwise vortex has its centre located just below the wake centerline. At some locations, we may identify separated peaks due to the poorly-defined clockwise vortices and their centres lie in similar lateral locations as the counterclockwise vortex on the upper side of the wake. The magnitudes of peak vorticity levels in the main clockwise vortex are always higher than those in its counterclockwise vortex partner on the lower side of the wake. The counterclockwise vortex on the upper side of the wake possesses slightly higher magnitudes than the main clockwise vortex.

According to the latest mode map of Morse and Williamson (2009), this flow case of our experiments falls close to the regime boundary of the 2S mode and inside the regime of the newly discovered $2P_O$ mode. However, the vortex pattern is different from the description of the $2P_O$ mode in Morse and Williamson (2009). We tend to describe this pattern as a young 2P mode in which the vortex of one sense of rotation cannot fully bifurcate into two vortices. This may be because the present value of A/D is just higher than that of the 2S mode and full transition into the 2P mode might require slightly higher cylinder oscillation amplitude.

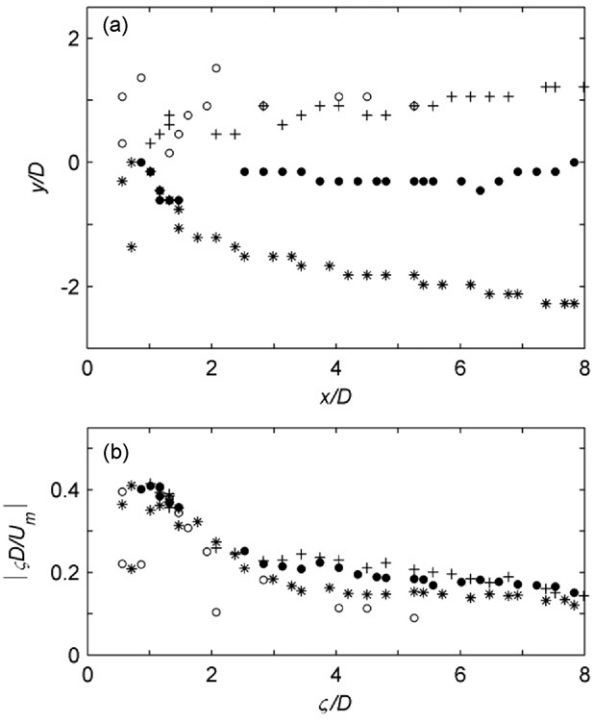

Fig. 10. Convection paths and peak vorticity levels of vortices in 2P mode: (a) locations of peak vorticity; (b) magnitudes of peak vorticity. Symbols: +, counterclockwise vortex of positive vorticity centred at $y>0$; *, counterclockwise vortex centred at $y<0$; ●, main clockwise vortex of negative vorticity centred at $y<0$; ○, clockwise vortex centred at $y>0$.

The incomplete bifurcation of the counterclockwise vortex is revealed from the phase-averaged flow patterns. We further investigate this feature in the instantaneous flow patterns of individual cylinder cycles. The instantaneous PIV flow fields in almost all the 30 cylinder cycles show the young 2P mode such as the example shown in Fig. 11(a). In 4 cycles, however, we can observe some degree of bifurcation of the elongated region of negative vorticity which leads to two counterclockwise vortices of better identities of separation. One example is shown in Fig. 11(b). Nevertheless, these vortices are never located at laterally distances as far as the clockwise vortices, as would be the case of a mature 2P mode.

Our earlier result in Fig. 3 suggests that in the P+S mode, the lateral oscillations of the cylinder govern the vortex formation mechanism more significantly than the uniform flow stream. In this section, it appears that the main mechanism for vortex formation in the 2S and 2P modes comes from the uniform cross-flow. Vortices are formed from the roll-up of the separation shear layers but the subsequent development is affected by the amplitudes of the lateral cylinder oscillations. When we use the concept of vortex formation distance of Jeon and Gharib (2004), the combination of U_0 and U_m should be used instead of just $\lambda = U_0T$. If you take a combined velocity of $(U_0^2 + U_m^2)^{1/2}$ in our two flow cases, the relative distance covered by the cylinder in one oscillation cycle would be $5.8D$ and $7.3D$, respectively. These distances are, respectively, about 1.2 and 1.5 times the suggested vortex formation distance of $4.8D$. This may provide a reason for the formation of one vortex of a given sense of rotation per cycle in the former 2S mode. In the latter flow case, the 1.5 times the natural vortex formation distance may be responsible for the shedding of two well-separated vortices of one sense of rotation and two still-connected vortices of the other sense in one cylinder oscillation cycle. If the cylinder oscillation amplitudes are larger, the ratio would become greater than 1.5 times and the well-established 2P mode would occur when the flow case moves well into the corresponding regime of the mode map.

3.3. Coherent and random vortex dynamics

In the preceding sections, we argue that the formation of vortex pattern is governed by the relative actions of the uniform flow stream and the lateral oscillations of the cylinder. In the 2S and 2P modes, the cylinder oscillates with low lateral velocities as compared to U_0. The vortex formation mechanism is mainly due to shear-layer separation of the

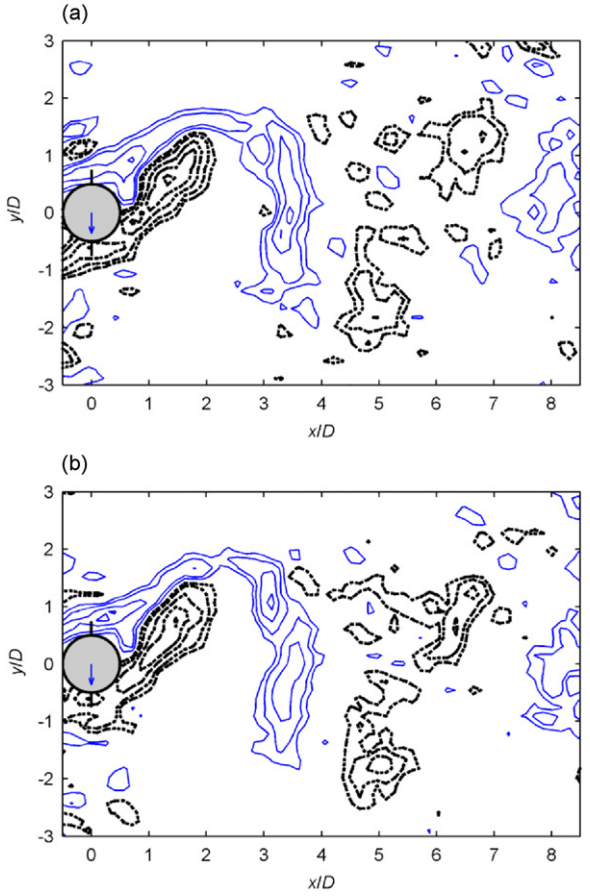

Fig. 11. Examples of instantaneous vortex patterns in 2P mode, at phase while cylinder moving downwards through neutral position. Vorticity contours at $\zeta D/U_m = \{\pm 0.05,\ \pm 0.1,\ \pm 0.2,\ \pm 0.3,\ \ldots\}$: (a) young 2P mode; (b) more mature 2P mode.

uniform flow and the cylinder motion acts as a perturbation to the wake flow, thus regulating or triggering the shedding of vortices from the cylinder (Ongoren and Rockwell, 1988a, b; Jeon and Gharib, 2001). At large cylinder oscillation amplitudes, that is fast U_m, vortex formation in the P+S mode is governed by the cylinder motion instead, and the uniform flow acts to convect the vortices downstream.

The synchronization of vortex pattern with cylinder motion can be investigated through the examination of the coherent and random components of the vortex dynamics using the phase-averaging technique (Reynolds and Hussain, 1972; Cantwell and Coles, 1983; Govardhan and Williamson, 2001). We adopt the triple decomposition method in which a flow quantity, $s(t)$, is decomposed into a time-averaged mean component, $\bar{s}$, a coherent and periodic component, $\tilde{s}$, and a random turbulent component, s'. The phase-locked averaging technique removes the last component and yields the mean and coherent components; $\langle s \rangle = \langle \bar{s} + \tilde{s} + s' \rangle = \bar{s} + \tilde{s}$. For brevity, we present here only the Reynolds normal stress due to lateral velocity component to show the vortex dynamics (Cantwell and Coles, 1983; Lam, 1996; Lam and Leung, 2005). Fig. 12 shows the coherent and random components of this stress for our three flow cases at the phase where the cylinder reaches its uppermost position. The stress components have been normalized using U_0^2 and are shown as $\tilde{v}\tilde{v}/U_0^2$ and $\langle v'v' \rangle / U_0^2$. When compared with Fig. 1, large values of coherent stress are produced at regions between successive vortices where fluid is induced to flow between them with very large lateral velocities. On the other hand, random stress components mainly occur near the vortex cores. If we compare Fig. 12 with the reported results for a stationary circular cylinder or bluff body in uniform cross-flow [e.g., Cantwell and Coles (1983), Lam (1996)], it is evident that the coherent components in the present flow are of much larger magnitudes than the random components. This implies that vortices behind our oscillating cylinder are arranged in a more regular and periodic pattern. It is also noted in Fig. 12 that the levels of both stress components increase from the 2S mode to the 2P mode and the P+S mode has much higher levels. This provides evidence that the levels of momentum transport are governed not only by U_0 but also by the cylinder movement as represented by U_m.

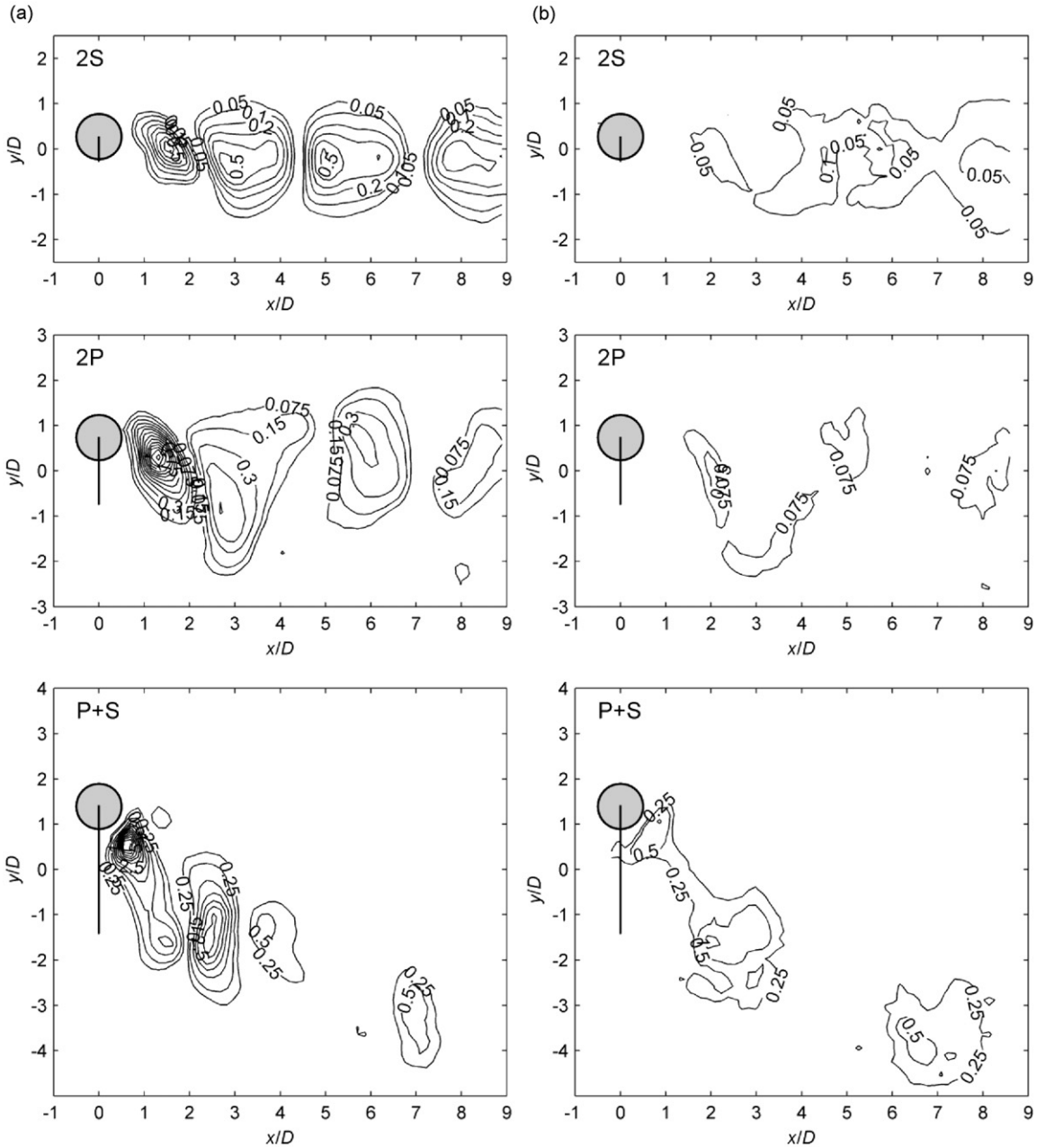

Fig. 12. Reynolds stress of lateral velocity fluctuations associated with phase-averaged flow field when cylinder reaches its extreme position for our 2S, 2P and P+S vortex modes: (a) coherent component: $\tilde{v}\,\tilde{v}/U_0^2$; (b) random component: $\langle v'v'\rangle/U_0^2$.

Fig. 13 shows the global mean values of the Reynolds stresses in Fig. 12, that is, the values averaged over all phases of the cylinder oscillation cycle. The high periodicity and regularity of the vortex pattern lead to a uniform and regular convection of the vortices in the wake at successive phases of the cylinder oscillation cycle. Thus, there are uniform high values of $\overline{\langle \tilde{v}\tilde{v}\rangle}/U_0^2$ along the paths of the vortices (Fig. 13(a)). In Fig. 13(b), randomness of the stress, $\langle \overline{v'v'}\rangle/U_0^2$, increases with more jitter as the vortex are convected downstream. The patterns of our 2S or 2P mode are similar to that reported for a stationary cylinder in uniform cross-flow [e.g., Cantwell and Coles (1983)] but in our case, the coherent component is much more important than the random component. There is almost no energies due to the random component of the Reynolds stress within the first $3D$ downstream of the cylinder, implying that the formation of the

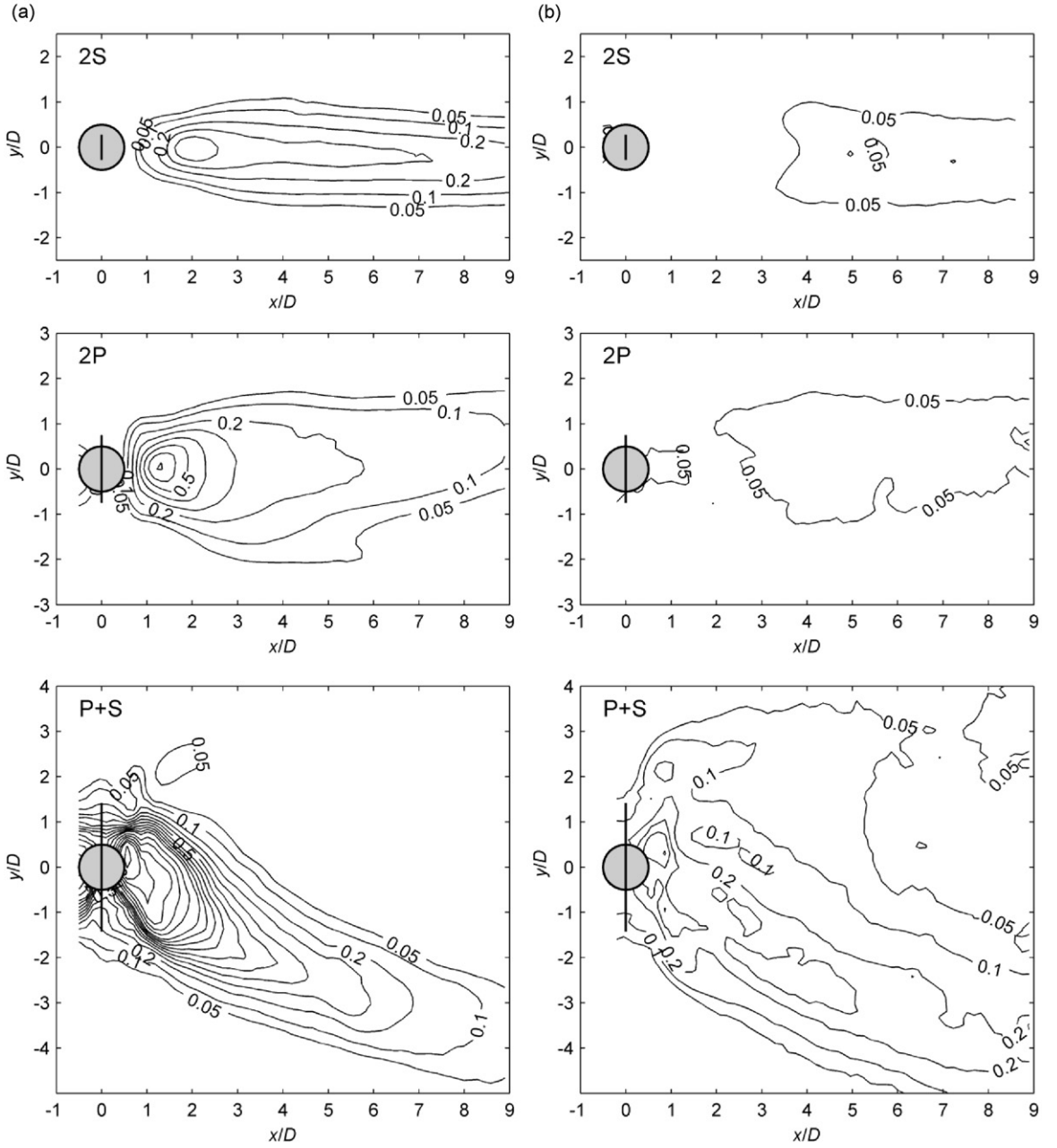

Fig. 13. Global mean Reynolds stress of lateral velocity fluctuations associated with vortices in our 2S, 2P and P+S vortex modes: (a) coherent component: $\overline{\langle \tilde{v}\tilde{v} \rangle}/U_0^2$; (b) random component: $\langle \overline{v'v'} \rangle / U_0^2$.

vortices are highly periodic. This is not the case for the P+S mode in which vortices are formed at different lateral positions of the cylinder strokes. The sum of the two components in Fig. 13 gives the total Reynolds normal stress.

4. Conclusions

In this paper, we attempt to investigate the mechanism of vortex formation and pattern behind a cylinder given lateral oscillations in the presence of a slow uniform flow stream. It is proposed that vortex formation can be caused

and affected by both the flow stream (of velocity U_0) and the relative flow due to the cylinder movement (which is measured by U_m, the maximum cylinder moving speed). Time-resolved PIV measurements are made for three flow cases and the phase-locked averaging technique is used to extract the flow field and vortex dynamics at successive phases in a cylinder oscillation cycle. By plotting the phase-averaged flow vectors relative to the moving cylinder, we are able to explore more clearly the connection between the development of the shear-layer vortices and the cylinder movement.

In the first two flow cases, the cylinder oscillates at a frequency close to the natural vortex shedding frequency of a stationary cylinder. It is found that the main mechanism for vortex formation is due to the uniform cross-flow which separates from the cylinder and forms shear layers of concentrated vorticity. The lateral oscillations of the cylinder affect the subsequent development of these shear-layer vortices and vortex shedding becomes synchronized with the oscillation cycle. The 2S mode is thus formed at smaller amplitudes of cylinder oscillations in which the distance covered by the cylinder, relative to the combined uniform flow and lateral flow relative to the moving cylinder, during the formation time of one vortex is around the natural vortex formation distance of $4.8D$, as suggested by Jeon and Gharib (2004). The vortices of the 2S mode are found to convect in the wake at locations very close to the wake centerline.

When the cylinder oscillation amplitudes become larger so that the relative distance covered by the cylinder in one cycle is rougher more than 1.5 times the natural vortex formation distance, the 2P mode vortex pattern occurs. The shear-layer vortex is stretched by the large lateral movement of the cylinder and bifurcates into two parts. The leading part is shed and pairs up with a preceding vortex of the opposite sense of rotation to become one vortex pair in that side of the wake. The trailing part of the stretched shear-layer vortex is shed at a later stage by the intrusion of the shear-layer vortex of the opposite sense of rotation from the other side of the cylinder. The later vortex will subsequently undergo stretching and bifurcation, leading to the next vortex pair on the other side of the wake. The 2P mode in our second flow case is in an early form in which the bifurcation of one shear-layer vortex does not occur completely so that two vortices are not fully separated.

Our P+S mode occurs at a low value of λ/D and we find a close connection of its vortex formation mechanism with that of a cylinder oscillating in an otherwise quiescent fluid ($\lambda/D=0$). The formation mechanism of a vortex street pattern of the later case at $8<\mathrm{KC}<16$, which is caused by the lateral oscillations of the cylinder, is found to be the key driving action for vortex formation in the P+S mode. A vortex is rolled up from the upstream side of the cylinder and develops during a cylinder stroke. Near the end of the stroke, it has migrated to the downstream side, partly due to the uniform cross-flow. For the first half of the returning cylinder stroke, the vortex continues to grow by attaching to the shear layer of the downstream side of the cylinder. Vortex shedding occurs near the middle of the stroke at which the vortex is under a stretching action from the previously shed vortex of the opposite sense of rotation. The main part of the shear-layer vortex is thus shed and pairs up with the previous shed vortex to form a vortex pair which is convected downstream as an inclined vortex street. The other and smaller part remains attached to the cylinder and is left behind and convected by the uniform flow as a single vortex when the cylinder reverses its moving direction.

In the P+S mode, the value of U_m is much higher than U_0, and in the middle part of a cylinder stroke the cylinder is moving at a speed higher than U_0. This explains why the vortex formation mechanism is governed by the lateral cylinder movement while the uniform flow stream mainly acts to convect the vortex pattern downstream, thus reducing the angle of inclination of the inclined vortex street to less than 45°. We find that the vorticity levels of the vortices scale better with U_m than U_0. The P+S mode is an asymmetric vortex pattern and leads to a net excess fluid circulation in the wake. This may be associated with a non-zero value of mean fluid force on the cylinder in the lateral direction.

We also investigate the coherent and random parts of momentum transport by the vortices in the wake. It is found that in all modes where vortex formation and development are governed by the combined action of the uniform flow and the cylinder oscillations, the vortex pattern is found to exhibit better regularity and periodicity.

Acknowledgement

The investigation is supported by a research grant (HKU7144/05E) awarded by the Research Grants Council of Hong Kong.

Appendix A. Supplementary material

Supplementary data associated with this article can be found in the online version at doi:10.1016/j.jfluidstructs.2010.03.007.

References

Bishop, R.E.D., Hassan, A.Y., 1964. The lift and drag forces on a circular cylinder oscillating in a flowing fluid. Proceedings of the Royal Society of London A 227, 51–75.

Cantwell, B., Coles, D., 1983. An experimental study of entrainment and transport in the turbulent near wake of a circular cylinder. Journal of Fluid Mechanics 136, 321–374.

Govardhan, R., Williamson, C.H.K., 2001. Mean and fluctuating velocity fields in the wake of a freely-vibrating cylinder. Journal of Fluids and Structures 15, 489–501.

Jeon, D., Gharib, M., 2001. On the circular cylinders undergoing two-degree-of-freedom forced motions. Journal of Fluids and Structures 15, 533–541.

Jeon, D., Gharib, M., 2004. On the relationship between the vortex formation process and cylinder wake vortex patterns. Journal of Fluid Mechanics 519, 161–181.

Lam, K.M., 1996. Phase-locked eduction of vortex shedding in flow past an inclined flat plate. Physics of Fluids 8, 1159–1168.

Lam, K.M., 2009. Vortex shedding flow behind a slowly rotating circular cylinder. Journal of Fluids and Structures 25, 245–262.

Lam, K.M., Dai, G.Q., 2002. Formation of vortex street and vortex pair from a circular cylinder oscillating in water. Experimental Thermal and Fluid Science 26, 901–915.

Lam, K.M., Hu, J.C., Liu, P., 2010. Vortex formation processes from an oscillating circular cylinder at high Keulegan–Carpenter numbers. Physics of Fluids 22, 015105.

Lam, K.M., Leung, M.Y.H., 2005. Asymmetric vortex shedding flow past an inclined flat plate at high incidence. European Journal of Mechanics B/Fluids 24, 33–48.

Liu, P., Hu, J.C., Lam, K.M., 2008. Vortex pattern of an oscillating circular cylinder in the presence of an ambient flow. In: Proceedings of Second International Symposium on Shallow Flows, Hong Kong.

Morse, T.L., Williamson, C.H.K., 2009. Fluid forcing, wake modes, and transitions for a cylinder undergoing controlled oscillations. Journal of Fluids and Structures 25, 697–712.

Obasaju, E.D., Bearman, P.W., Graham, J.M.R., 1988. A study of forces, circulation and vortex pattern around a cylinder in oscillating flow. Journal of Fluid Mechanics 196, 467–494.

Ongoren, A., Rockwell, D., 1988a. Flow structure from an oscillating cylinder. Part 1. Mechanisms of phase shift and recovery in the near wake. Journal of Fluid Mechanics 191, 197–223.

Ongoren, A., Rockwell, D., 1988b. Flow structure from an oscillating cylinder. Part 2. Mode competition in the near wake. Journal of Fluid Mechanics 191, 225–245.

Reynolds, W.C., Hussain, A.K.M.F., 1972. The mechanics of an organized wave in turbulent shear flow. Part 3. Theoretical models and comparisons with experiments. Journal of Fluid Mechanics 54, 263–288.

Tatsuno, M., Bearman, P.W., 1990. A visual study of the flow around an oscillating circular cylinder at low Keulegan–Carpenter numbers and low Stokes numbers. Journal of Fluid Mechanics 211, 157–182.

Willert, C.E., Gharib, M., 1991. Digital particle image velocimetry. Experiments in Fluids 10, 181–193.

Williamson, C.H.K., 1985. Sinusoidal flow relative to circular cylinders. Journal of Fluids and Structures 15, 141–147.

Williamson, C.H.K., Roshko, A., 1988. Vortex formation in the wake of an oscillating cylinder. Journal of Fluids and Structures 2, 355–381.